Int. J. Electrochem. Sci., 8 **(2013)** 80 - 99

International Journal of
ELECTROCHEMICAL
SCIENCE
www.electrochemsci.org

Electrochemical deposition of SERS active nanostructured silver films

Renáta Oriňáková[1*], *Lenka Škantárová*[2], *Andrej Oriňák*[1], *Jakub Demko*[1], *Miriam Kupková*[3], *Jan T. Andersson*[4]

[1] Department of Physical Chemistry, Faculty of Science, P.J. Šafárik University, Moyzesova 11, SK-04154 Košice, Slovak Republic, European Union
[2] Department of Analytical Chemistry, Faculty of Science, Comenius University, Mlynská Dolina, SK-842 15 Bratislava 4, Slovak Republic, European Union
[3] Institute of Materials Research, Slovak Academy of Science, Watsonova 47, SK-04353 Košice, Slovak Republic, European Union
[4] Institute of Inorganic and Analytical Chemistry, University of Münster, Correnstrasse 30, D-48149 Münster, Germany, European Union
[*] E-mail: Renata.Orinakova@upjs.sk

Received: 31 July 2012 / *Accepted:* 31 August 2012 / *Published:* 1 January 2013

An electrochemical multiple scan cyclic voltammetry (CV) method was used to prepare surface-enhanced Raman scattering (SERS) active silver island films to investigate the effect of potential scan rate and number of CV scans on the SERS performance. The SERS enhancement capability is particle size and distribution as well surface profile amplitude dependent with an optimal potential scan rate of 100 mV/s and 30 CV scans at the experimental conditions used. Scanning electron microscopy and optical profilometry investigation reveal that the highest SERS effect was associated with the homogenously distributed uniform size aggregates merged to interconnecting network. The enhancement factor for Rhodamine 6G (R6G) adsorbed on the SERS-active Ag film was estimated to be 3.7×10^{12} and a detection limit of about 5×10^{-16} mol/l was reached.

Keywords: Electrochemical Deposition, Cyclic Voltammetry, Surface-Enhanced Raman Scattering, Ag Island Films, Enhancement Factor

1. INTRODUCTION

The technique of surface enhanced Raman spectroscopy (SERS) is a particularly sensitive and selective analytical tool for the detection of low-concentrations of analytes adsorbed on noble metal nanostructures [1-5], sometimes even achieving single-molecule sensitivity [2, 6, 7]. SERS occurring

on nanostructured metallic surfaces provides a powerful means of obtaining vibrational information on adsorbate–surface interactions in view of its unique sensitivity and excellent frequency resolution from the large increase in scattering [3-5, 7-9]. The detection of single molecules elevated SERS to the very restricted group of techniques able to attain this ultimate limit of detection and gave a new direction to the SERS research field [7]. SERS is widely applied to the study of the structure and orientation of molecules at Cu, Ag and Au surfaces [1, 10]. The surface enhancement is highly surface selective so the technique is sensitive to molecules adsorbed at, or very close to the substrate surface. Moreover, the Raman cross section for water is low so that SERS can be easily used to study substrates in aqueous solution [1]. SERS has grown to become a very active field of research in several areas of materials and analytical sciences [7].

The mechanism of SERS, as it is now widely accepted, consists of two major components contributing to the overall SERS effect: electromagnetic (EM) and chemical (CHEM) enhancement [3-5, 10-12]. The former arises from the enhancement of the electromagnetic field at the analyte location due to the occurrence of localized surface plasmon resonance (LSPR) [3, 4, 7, 11]. The local field can be enhanced to a far greater extent when neighbouring nanofeatures interact with each other over distances in the order of 1–2 nm [7, 13]. The regions of highly enhanced local electromagnetic fields are called "SERS hot spots". CHEM enhancement takes place only if molecules are in contact with the surface directly, and it is associated with the charge transfer between the metal and adsorbate at atomic-scale roughness features [3-5, 11]. The most common of the chemical models assume the appearance of new electronic states due to chemisorption [7]. This is poorly understood in comparison to the EM enhancement [4, 5]. Of these two the EM contribution is usually the more significant and is not adsorbate specific [1, 12]. The magnitude of the EM enhancement is highly dependent on the surface morphology and the precise shape of the roughness features at the metal surface as well on the plasmon absorption of the SERS substrate [1, 7, 10, 12, 14].

An average value for the SERS enhancement is around 10^6 but the localized enhancement may reach peaks of 10^{10} at certain highly efficient sub-wavelength regions of the surface [7]. The generation and intensity of Raman signals are determined by the surface morphology and structure of the substrates [1, 7, 8, 12]. Thus, considerable efforts have been directed toward the optimization of SERS enhancement via the size- and shape-controlled physical and chemical properties of the SERS active substrates [12]. One of the major challenges in the field of SERS is the difficulty in producing efficient SERS substrates with good stability, at low cost and high enhancement factors, with reproducibility and uniformity over the whole substrate. It is also desirable that the substrates are easy to fabricate and store [2, 3, 9].

The original substrates for SERS were electrochemically roughened metal electrodes [7, 15, 16]. Currently, there are many kinds of SERS-active substrates used in a wide range of SERS applications. These include the use of grating structures [17], colloidal particle arrays [18, 19], and geometrically structured metal surfaces [20]. Of special interest is the synthesis of noble-metal (Au, Ag and Cu) nanoparticle patterns with controllable particle size and shape, because such nanoparticle patterns offer the possibility of developing various functional devices with optical, sensing, and electrical properties [6, 7, 11, 12].

In preparing metal island films on substrates for SERS studies, various techniques have been developed. They include electron beam lithography [21], microcontact printing [22], sputtering coating [23], vacuum evaporation deposition [24], self-assembly [25], laser deposition [26], electrochemical deposition [27], chemically etching methods [28], and so on. Recent investigations have highlighted electrodeposition as an attractive approach for the preparation of nanostructured materials. Electrodeposition, which does not require complex equipment, provides a cost-effective method for the preparation of nanocrystalline and nanophase metallic materials either as coatings or as freestanding objects even in complex shapes (foils, wires, electroforms). The low processing temperature minimizes interdiffusion or chemical reaction. The film thickness can be accurately controlled by monitoring the consumed charge. Composition and defect chemistry can be controlled by electrical and fluid-dynamic means. Deposition rates of the order of several tens of microns per hour can be routinely achieved [29, 30]. A controllable and reproducible surface roughness can be generated through control of the electrochemical oxidation–reduction cycles procedure [4, 5].

It has been established that metallic silver is an excellent material for SERS [3, 5, 6, 8-10, 15, 17, 25, 31]. Ag arrayed nanostructure has been extensively studied and become one of the best established systems [3, 10, 32]. Recently, SERS effects of various nanostructures, for example, Ag nanowire bundles [8], Ag nanorod arrays [10, 14], Ag dendritic structures [31, 33], flowerlike Ag nanostructures [34] and nanoparticles [12, 32] were reported.

In this work, the silver island films were produced using electrodeposition onto stainless steel substrates by cyclic voltammetry (CV). The morphology of substrates was changed through tuning the scan rate of the applied potential and the number of scans. The Raman scattering enhancement efficiency of the prepared surfaces was investigated by SERS measurements of Rhodamine 6G (R6G) as a reference molecule. The textural and topographical properties of the Ag nanoparticle substrate were correlated with the corresponding enhancement factor to determine the factors that could improve the design of Ag nanoparticle SERS active substrates.

2. EXPERIMENTAL PART

2.1. Electrochemical deposition of Ag island films

Silver island films were electrochemically synthesized by multiple scan CV using an electrolyte containing 0.1 mol/l KNO_3, 0.1 mol/l KCN and 0.01 mol/l $AgNO_3$ (pH = 10.25) in a conventional three-electrode cell controlled by an Autolab PGSTAT302N (Metrohm) at room temperature. A sheet of stainless steel with a bare surface area of 1 cm^2, a 0.56 cm^2 platinum sheet, and an Ag/AgCl/3 mol/l KCl electrode were employed as the working, counter and reference electrodes, respectively. The working electrode was typically cycled for 10 – 40 cycles between –700 and –1550 mV (vs. Ag/AgCl/3 mol/l KCl), beginning at –700 mV, with scan rate 50 – 250 mV/s in order to affect electrodeposition. The electrolyte solution was degassed by nitrogen purging.

2.2 Surface morphology of Ag island films

The morphology of the samples was characterized ex situ using a scanning electron microscope JEOL JSM-7000F (Japan). To better illustrate the surface topography, an optical confocal profilometer Plu NeoX (Sensofar, Spain) was used.

The particle size distribution histogram for each sample was calculated by analyzing 300 - 500 particles from SEM images taken at different regions of the sample in order to obtain particle Feret's diameter (also known as the caliper length).

2.3. SERS analysis of Ag island films

Raman spectra were obtained using an i-Raman® instrument (B&W Tek). Excitation was provided by a 532.1-nm Nd:YAG laser. The laser power at the sample was approximately 9 mW. The acquisition time for each accumulation was 5 s.

For SERS measurement, the prepared SERS-active Ag films were tested using R6G dye, due to its high Raman scattering cross-section for SERS. The structural formula of R6G is given in Fig. 1. For each test, 1 µl of the 5.10^{-4} mol/l (unless otherwise stated) ethanol R6G solution was dropped onto the SERS substrate and dried naturally. The desired concentration was prepared by precision diluting an accurate volume portion of stock solution by electronic microsyringes (eVol, SGE Analytical) to the final volume.

A total of ten measurements were made on each sample, at different locations, to compute the mean and standard deviation values of reported SERS intensities.

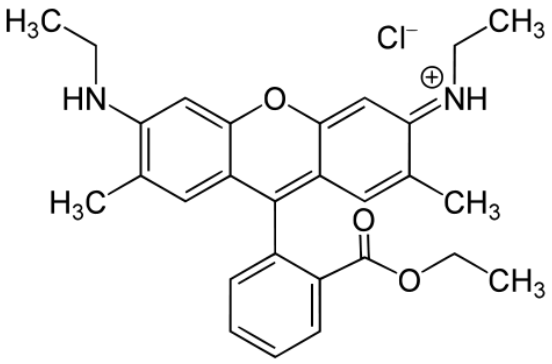

Figure 1. The structural formula of Rhodamine 6G ($C_{27}H_{29}ClN_2O_3$).

2.4. Chemicals

All chemicals were of analytical grade and solutions were freshly prepared. The chemicals were purchased from Alfa Aesar GmbH (Germany) and used without further purification.

3. RESULTS AND DISCUSSION

3.1. Preparation of Ag island films

Silver island films were electrochemically synthesized by multiple scan CV using an electrolyte containing 0.1 mol/l KNO_3, 0.1 mol/l KCN and 0.01 mol/l $AgNO_3$ on a stainless steel substrate. A low concentration of $AgNO_3$ (0.01 mol/l) is favourable for the deposition of nanosized layers. An excess of KCN (0.1 mol/l) in the electrolyte is required to avoid a precipitate formation. The cyclic voltammograms for the 0.1 mol/l KNO_3 supporting electrolyte alone and the supporting electrolyte containing 2×10^{-5} mol/l and 5.5×10^{-5} mol/l $AgNO_3$ on a stainless steel electrode are shown in Fig. 2. The voltammetric curve of the supporting electrolyte exhibits almost constant currents to the onset of hydrogen evolution at a potential of ca. -1200 mV. On the other hand, a sharp current increase starting at about -1050 mV was registered on cyclic voltammograms in the presence of $AgNO_3$. The observed rapid cathodic current increase on the polarisation curve corresponds to the potential at which Ag starts to nucleate. The hydrogen evolution commences simultaneously with the silver nanoparticle electrodeposition with a further shift to more negative potentials. During the reverse scan, an oxidation peak was observed on the anodic part of the polarisation curves at about -550 mV, corresponding to the dissolution of deposited Ag island films. The higher cathodic and anodic currents and the onset of reduction at the most positive potential were detected at higher Ag concentration. This behaviour can be explained by the diffusion character of the process. At much higher Ag concentration applied for the subsequent electrodeposition of Ag island films this diffusion control may be considerably reduced.

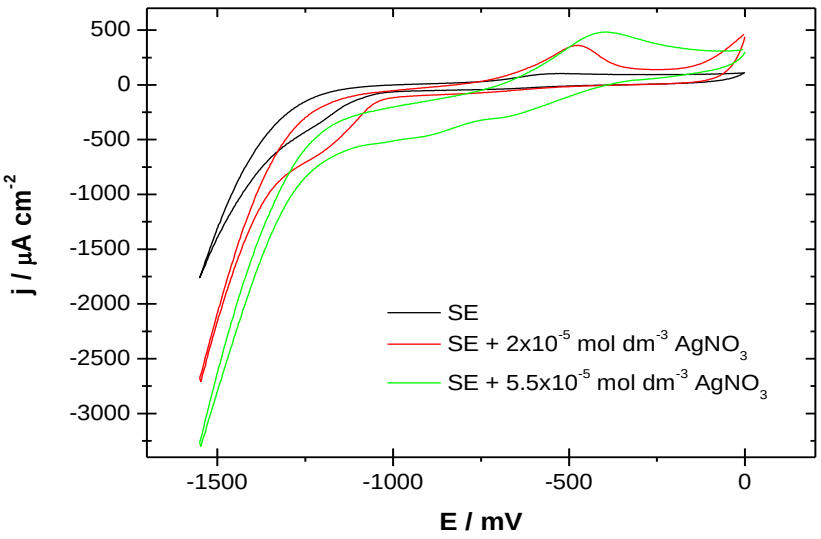

Figure 2. Polarisation curves obtained in 0.1 mol/l KNO_3 supporting electrolyte (SE) alone and supporting electrolyte containing 2×10^{-5} mol/l and 5.5×10^{-5} mol/l $AgNO_3$ on a stainless steel electrode at 25 mV/s (first cycle). The working electrode was polarised in the potential range from 0 V to −1.6 V and than back to 0 V (vs. Ag/AgCl/3 mol/l KCl).

From these measurements, the desired range of the deposition potential was selected between -700 mV and -1550 mV to involve an initial cathodic deposition step during which Ag nanoparticles are formed onto the working electrode as well a subsequent short anodic dissolution step during which the deposited Ag nanoparticles are partially dissolved. The morphology of substrates was affected by the scan rate of the applied potential and the number of scans.

3.2. Characterisation of Ag island films

Effect of CV scan number. The morphology of silver structures electrodeposited onto a stainless steel working electrode was found to be highly dependent on the number of applied CV scans. Figures 3(a) – (g) show the SEM images of the Ag island films deposited after 10, 15, 20, 25, 30, 35 and 40 CV scans, respectively. These images are representative of many images taken at different regions of the substrate and at a number of magnifications. The surface of the working electrode is decorated with spherical silver nanoparticles and clusters with varying size distributions (ca. 90 – 500 nm in diameter) which consist of aggregated smaller crystallites. Lower magnification images revealed the nanoparticle and cluster beads like arrays. Both the size and the density of the Ag nanoparticles increased with increasing number of deposition cycles (to ca. 900 nm in diameter). When the number of CV scans is increased to 35 and 40, the tendency of nanoparticles to coalesce become more pronounced and the formation of tighter and larger rod-like structures (of ca. 1.5 μm wide and 4.5 μm long) is favored over smaller more discrete chain structures.

Particle size distribution histograms (Fig. 4) were calculated from the respective SEM images. The Feret's diameter, expressing the longest distance between any two points along the particle or aggregate, increased with increasing number of CV scans. At lower CV scan number (Figs. 4(a) - (d)), particles with the Feret's diameter less than 500 nm predominated but at higher numbers (Figs. 4(e) - (g)) the fraction of small particles decreased and the amount of larger particles (over 2 μm) increased.

Fig. 5 demonstrates the effect of the applied CV scan number for electrochemical deposition of silver structures on stainless steel substrates by multiple scan CV method on the corresponding SERS performance at a potential scan rate of 100 mV/s. The peaks are characteristics of R6G in a Raman spectrum. The peak at ca. 612 cm^{-1} is assigned to the C–C–C ring in-plane vibration mode. The peak at ca. 775 cm^{-1} is assigned to the C–H out-of-plane bend mode. The peaks at ca. 1126 and 1185 cm^{-1} are assigned to the C–H in-plane bend mode. The peaks at ca. 1313 and 1577 cm^{-1} are assigned to the N–H in-plane bend modes. The peaks at ca. 1362, 1508 and 1650 cm^{-1} are assigned to the C–C aromatic stretching vibrations of R6G molecule [4, 5, 35 - 37].

The spectra (a–g) in Fig. 5 show that the optimum number of CV scans for obtaining the strongest SERS effect at fixed potential scan rate is 30 (spectrum e). The SERS spectrum of R6G adsorbed on the Ag nanoparticle film prepared after 30 CV scans exhibits approximately 5 times higher intensity of the strongest peak in the Raman spectrum (at 612 cm^{-1}) than that of R6G adsorbed on the other Ag films (Table 1). The Raman intensity decrease for large number of CV scans (>30) may be due to the aggregation state of Ag nanoparticles is not very capable of creating a great deal of SERS-active ‘‘hot spots’’.

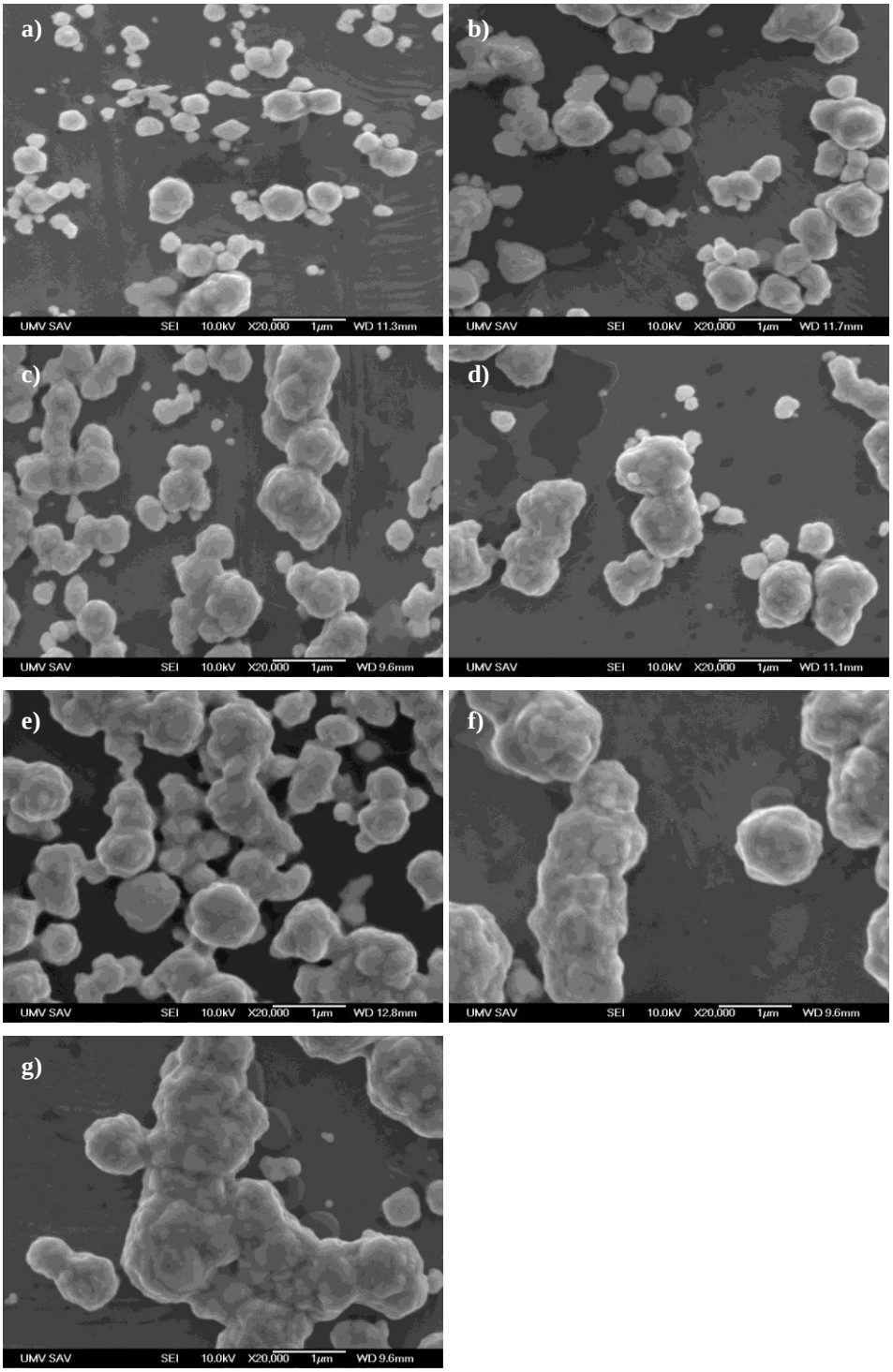

Figure 3. Representative SEM images of different Ag island films deposited on stainless steel substrates by multiple scan CV using an electrolyte containing 0.1 mol/l KNO_3, 0.1 mol/l KCN and 0.01 mol/l $AgNO_3$ between −700 mV and −1550 mV (vs. Ag/AgCl/3 mol/l KCl) at potential scan rate 100 mV/s after different number of CV scans: a) 10; b) 15; c) 20; d) 25; e) 30; f) 35; g) 40.

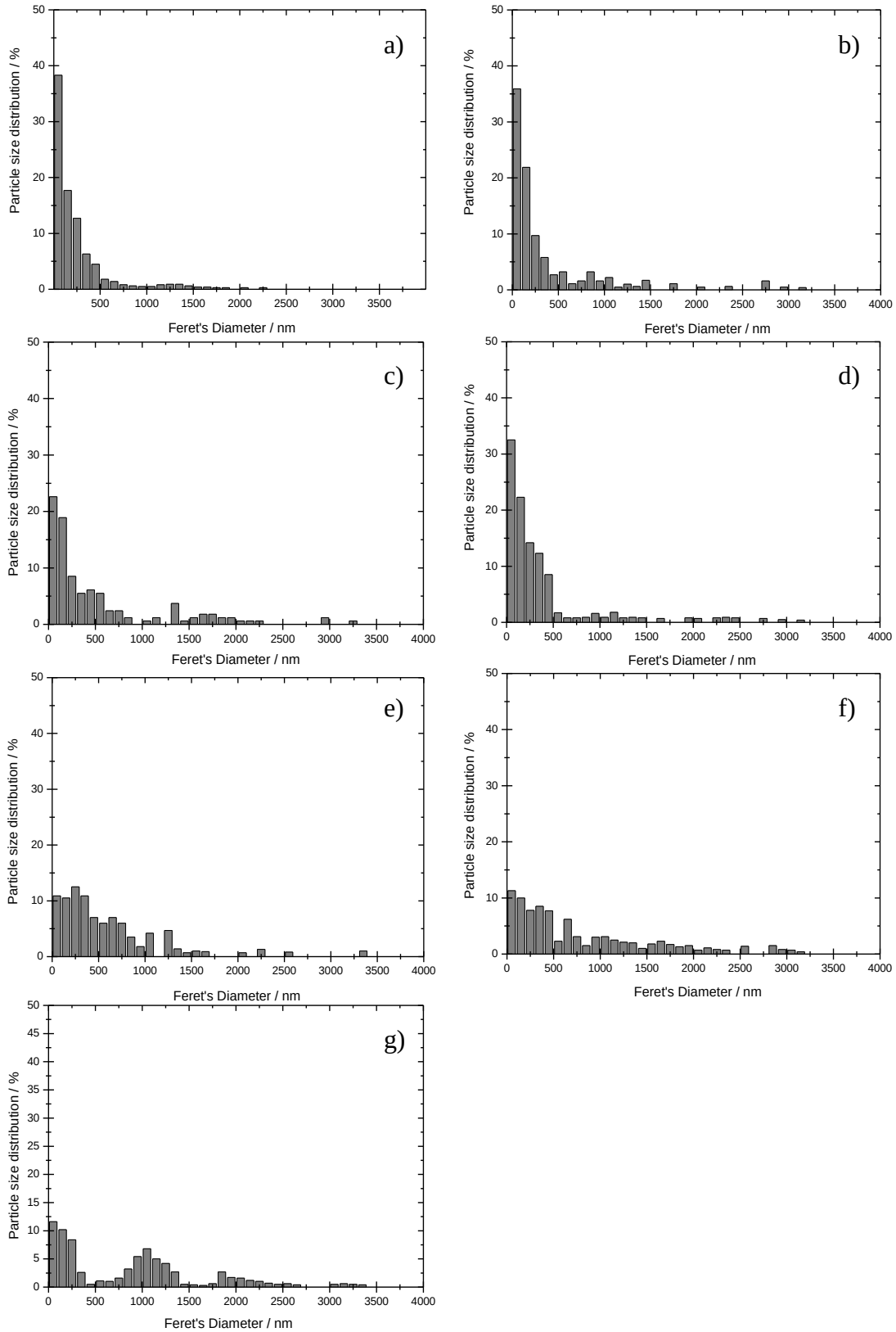

Figure 4. Histograms of nanoparticle size distribution of different Ag island films deposited on stainless steel substrates after different number of CV scans: a) 10; b) 15; c) 20; d) 25; e) 30; f) 35; g) 40. All other conditions are similar as in Fig. 3.

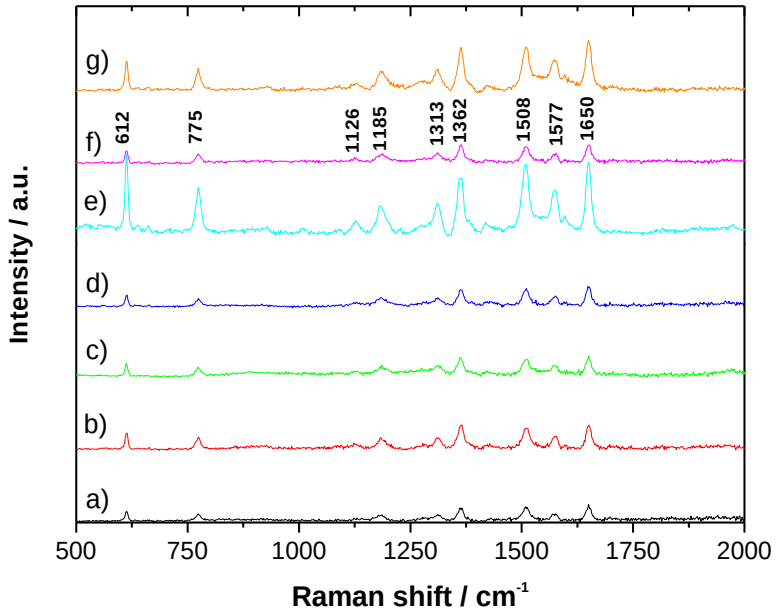

Figure 5. Representative SERS spectra of 5×10^{-4} mol/l R6G adsorbed on different Ag island films prepared by multiple scan CV at potential scan rate 100 mV/s after different number of CV scans: a) 10; b) 15; c) 20; d) 25; e) 30; f) 35; g) 40.

To assess the uniformity and reproducibility of SERS signals, the mean value and relative standard deviation (*RSD*) of the Raman intensity of the carbon skeleton stretching modes were calculated. The mean intensity and standard deviation of the main Raman vibrations of R6G adsorbed on Ag films deposited after different number of deposition cycles for the C–C–C ring in-plane vibration mode and the aromatic C–C stretching modes (612, 1362, 1508, and 1650 cm^{-1}), which were obviously enhanced at all spots, are summarised in Table 1. The less than 20% *RSD* variation of the four bands for the Ag nanoparticle film prepared after 30 CV revealed clearly the high reproducibility of the substrate [38].

Table 1. Values of the mean intensity (*MI*) and relative standard deviation (*RSD*) of the Raman intensity of the main Raman vibrations (612, 1362, 1508, and 1650 cm^{-1}) of R6G adsorbed on the Ag island film prepared at potential scan rate 100 mV/s after different number of CV scans.

Number of CV scans	612 cm^{-1}		1362 cm^{-1}		1508 cm^{-1}		1650 cm^{-1}	
	MI (a.u.)	*RSD* (%)	*MI* (a.u.)	*RSD* (%)	*MI* (a.u.)	*RSD* (%)	*MI* (a.u.)	*RSD* (%)
10	2491	28.4	3811	32.3	3914	28.3	4113	33.8
15	4367	25.2	6404	26.4	5380	21.2	6146	28.0
20	3515	27.5	4938	28.7	4733	30.2	5488	27.3
25	2949	20.2	4884	24.6	5240	26.0	5386	20.0
30	19385	15.8	13331	17.4	16485	15.4	17504	15.5
35	2911	33.0	4582	27.4	4027	31.9	4739	29.3
40	7838	33.4	10997	31.9	10690	30.9	12469	29.8

As observed by SEM, the best distribution as well uniformity of nanoparticle size was observed for the corresponding Ag island film (prepared after 30 CV scans, Fig. 3e). The size dispersion of Ag aggregates was lowest (500 – 900 nm in diameter) as compared to other samples, without very small particles and very large clusters. Moreover, the highest density and coverage can be seen for the corresponding Ag film. The interconnected aggregates form a porous structure, which makes the nanoparticle film surface very rough.

Effect of potential scan rate. To study the morphology of the electrodeposited Ag island films at various potential scan rates, the number of CV scans was kept constant as 30 deposition cycles.

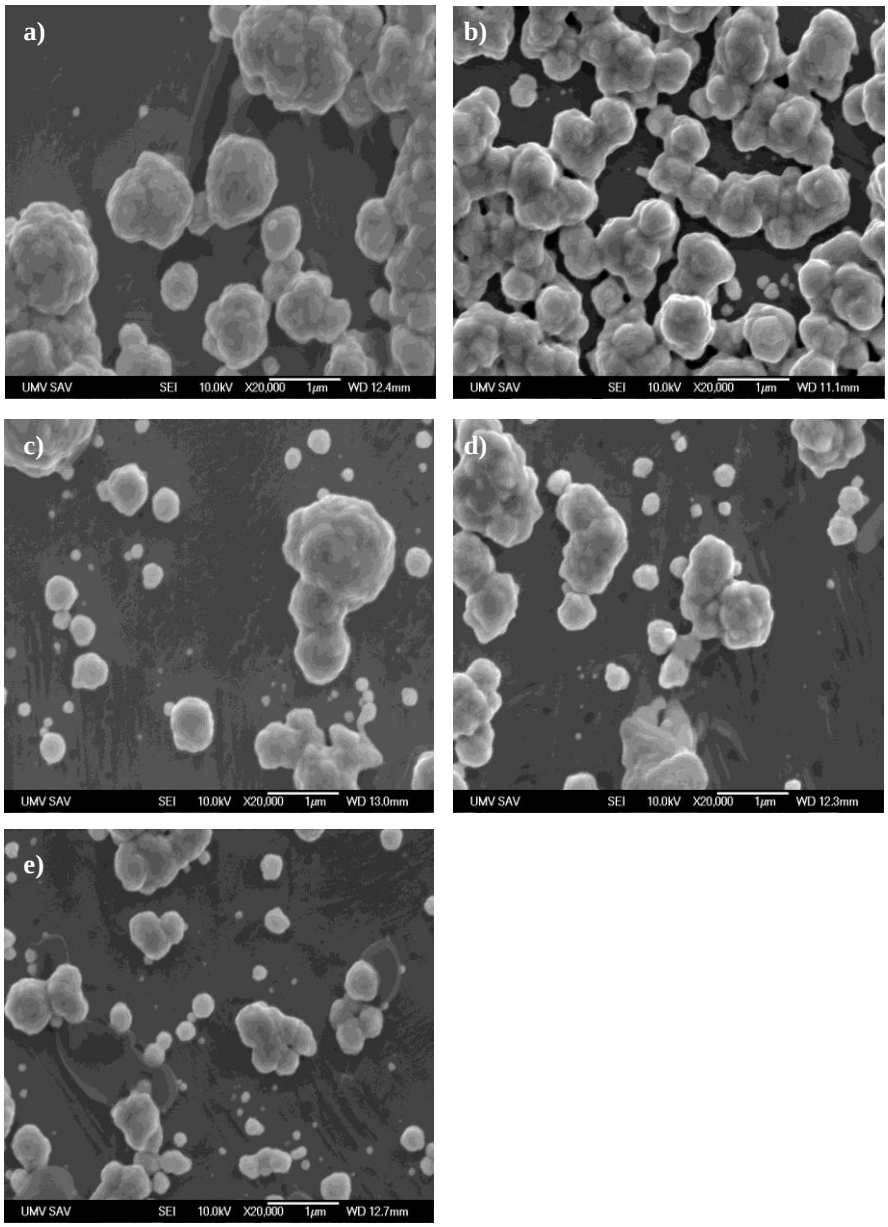

Figure 6. Representative SEM images of different Ag island films deposited on stainless steel substrates after 30 cycles at different potential scan rate: a) 50 mV/s; b) 100 mV/s; c) 150 mV/s; d) 200 mV/s; e) 250 mV/s. All other conditions are similar as in Fig. 3.

Figures 6(a) – (e) show representative SEM images of the Ag island films deposited at potential scan rates of 50, 100, 150, 200 and 250 mV/s, resp. With an increase in potential scan rate, the spherical nanoparticles and clusters become smaller and less aggregated. Moreover, the lower coverage of working electrode with Ag nanostructures was observed when the scan rate was increased. The time of deposition shortens with a rise in scan rate. The formation of Ag nanoparticles and aggregates involves two competitive processes: growth versus formation of new particles. At lower potential scan rates, the rate of the growth is slightly higher than that of formation. With increasing scan rate, the rate of formation increases while the rate of growth decreases. As the potential scan rate increases, the particle and cluster formation dominates. In consequence, as the scan rate increase from 50 to 250 mV/s, the number of small particles (90 – 270 nm in diameter) increased, the diameter of the aggregates decreased (from ca. 900 nm to 500 nm in diameter) and the size dispersion becomes broader.

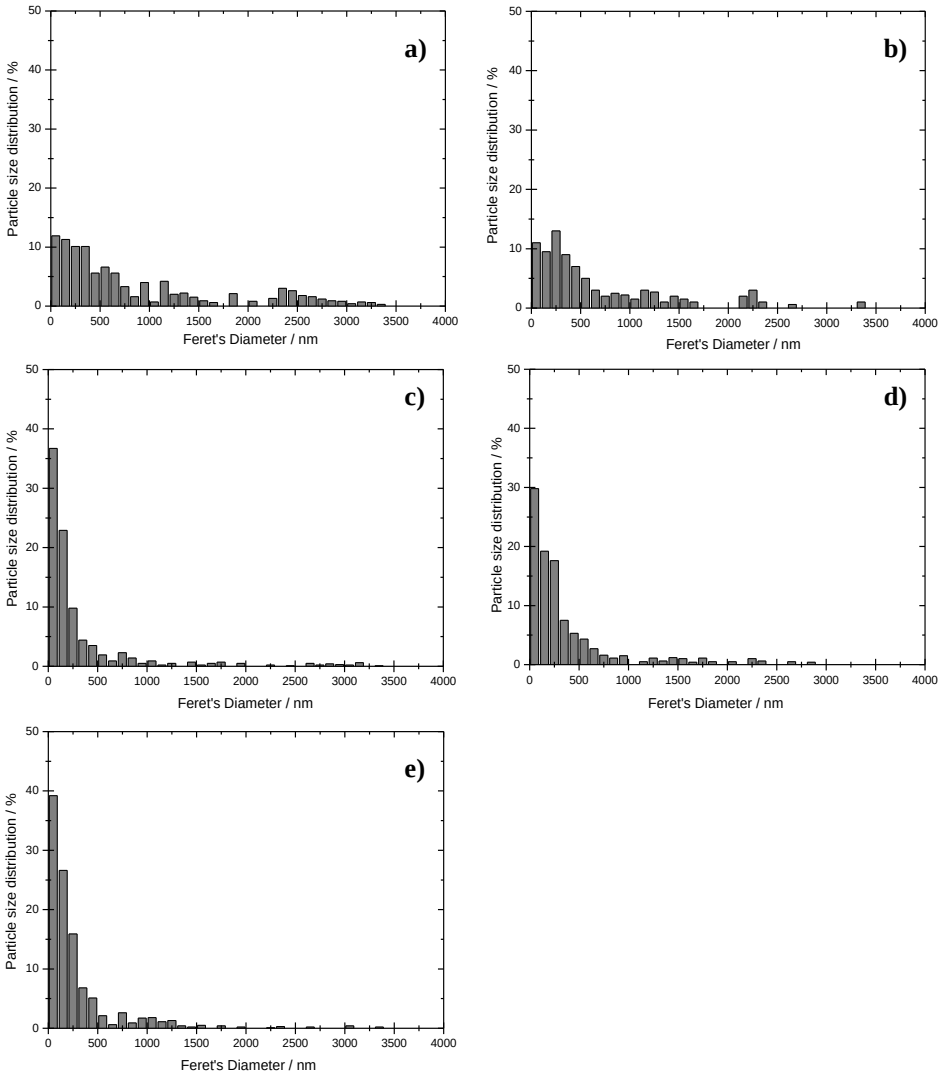

Figure 7. Histograms of nanoparticle size distribution of different Ag island films deposited on stainless steel substrates after 30 cycles at different potential scan rate: a) 50 mV/s; b) 100 mV/s; c) 150 mV/s; d) 200 mV/s; e) 250 mV/s. All other conditions are similar as in Fig. 3.

Figure 7 shows the particle size distribution of Ag nanoparticles produced at different potential scan rates, corresponding to Fig. 6. It can be seen that the Feret's diameter of the nanoparticles decreased with increasing scan rate. The number of particles in the range between 2 and 3 μm decreased and number of small particles with the Feret's diameter under 500 nm increased.

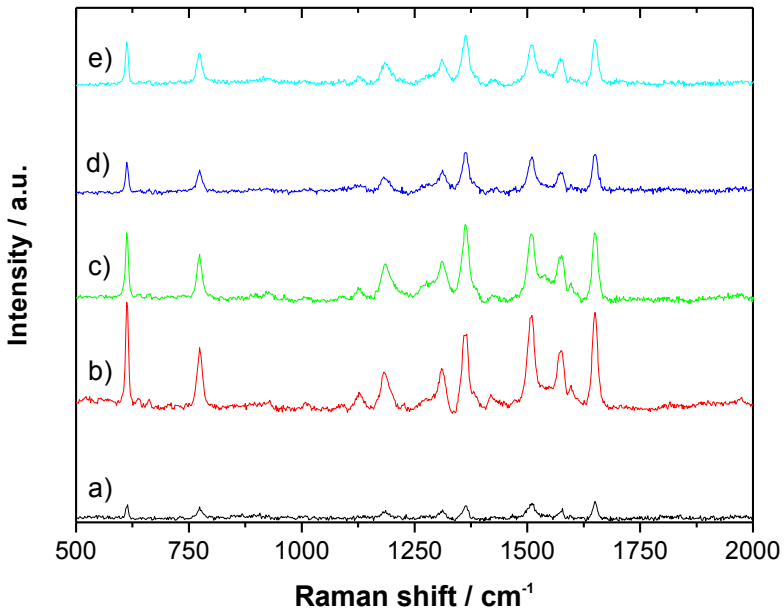

Figure 8. Representative SERS spectra of 5×10^{-4} mol/l R6G adsorbed on different Ag island films prepared by multiple scan CV after 30 cycles at different potential scan rate: a) 50 mV/s; b) 100 mV/s; c) 150 mV/s; d) 200 mV/s; e) 250 mV/s.

Fig. 8 shows the influence of the increasing potential scan rate on the corresponding SERS effect for Ag nanoparticle film electrodeposition from 50 to 250 mV/s. A significant increase in the Raman intensity was detected for the first increment of potential scan rate from 50 to 100 mV/s. However, a gradual decrease in the intensity of the signal was observed with a further increase of potential scan rate. Therefore, the maximum SERS activity was observed on the Ag island nanoparticle film deposited at 100 mV/s.

The mean intensity and standard deviation of the main Raman vibrations (612, 1362, 1508, and 1650 cm^{-1}) of R6G adsorbed on Ag films deposited at different potential scan rates are summarised in Table 2. The best reproducibility and uniformity of the SERS intensity was obtained for the Ag film deposited at 100 mV/s. Better surface uniformity clearly generated a more reproducible SERS signal. Nevertheless, all prepared Ag nanoparticle film provided acceptable reproducibility (better than 40%).

From the SEM images of the Ag nanoparticle films prepared at elevated potential scan rates (Fig. 6), it can be seen clearly that the highest density of Ag island films on the working electrode surface, best distribution and low size dispersion of Ag particles was observed for Ag film deposited at 100 mV/s. The uniform aggregates merge together to form an interpenetrating network. It indicates that the observed highest activity of the mentioned substrate can be related to the resulting overall porous-like structure.

Table 2. Values of the mean intensity (*MI*) and relative standard deviation (*RSD*) of the Raman intensity of the main Raman vibrations (612, 1362, 1508, and 1650 cm^{-1}) of R6G adsorbed on the Ag island film prepared after 30 cycles at different potential scan rate.

Potential scan rate	612 cm^{-1}		1362 cm^{-1}		1508 cm^{-1}		1650 cm^{-1}	
	MI (a.u.)	*RSD* (%)	*MI* (a.u.)	*RSD* (%)	*MI* (a.u.)	*RSD* (%)	*MI* (a.u.)	*RSD* (%)
50	2084	27.9	2372	30.1	3069	29.1	3392	25.2
100	19445	18.2	14586	17.9	17649	17.2	17735	16.8
150	12319	30.2	13959	29.4	12299	29.6	12460	29.9
200	5304	36.6	7303	34.4	6370	34.3	6960	36.4
250	7643	31.6	8952	31.2	7340	32.0	8369	32.1

It can be concluded that the signal intensity was significantly improved once the isolated structures become peripherally connected to the uniformly distributed open network of aggregates (ca. between 500 - 900 nm in diameter). Small discrete nanoparticles or clusters as well as large rod-like aggregates, which usually are randomly distributed and poly dispersive, were not susceptible to such a high Raman activity enhancement.

The spacing information obtained from the SEM micrographs was supplemented by the topographical data of surface features by means of optical profilometry. The amplitude parameters describe the deviations in height of a profile. In this study, the standard roughness parameter usually associated with the optical properties of surfaces was calculated. Root mean square (*RMS*) roughness is the root mean square average of all measured points from the center line. It represents the standard deviation of the profile heights and is mainly used in the statistical evaluation of a profile. Surface profile roughness (*Ra*), or surface area roughness (*Sa*) is the most commonly used roughness parameter. It describes the arithmetic average of all measured points from the center line (e.g. mean value) of a profile or surface area. It strongly averages the data and therefore is very robust against outliers. On the other hand, it is not very sensitive to peaks and grooves. In this regard *RMS* is more sensitive than *Ra* (*Sa*).

Both amplitude parameters (*RMS* and *Sa*) were found to correlate inversely with the intensity value of R6G adsorbed on the Ag island nanoparticle film peak at 612 cm^{-1}. Figs. 9 and 10 show the correlation curves of the surface area roughness (*Sa*), the root mean square (*RMS*) and the corresponding SERS effect with the increasing number of CV scans and with the increasing potential scan rate, respectively. Minimal values of amplitude parameters correspond to maximal SERS intensity values. When the value of *RMS* decreased to ca. 67 nm and the value of Sa to ca. 51 nm, the intensity of the most intensive Raman peak at 612 cm^{-1} increased up to 2×10^4 a.u., which is attributed to the best dispersion and most uniform size of Ag particles as well as to the appropriate aggregation of Ag nanoparticles and the interconnection of some aggregates.

These results indicate that the high SERS activity is associated with the low amplitude roughness of the surface area. On the contrary, the high amplitude of profile heights hinders the SERS activity of the surface.

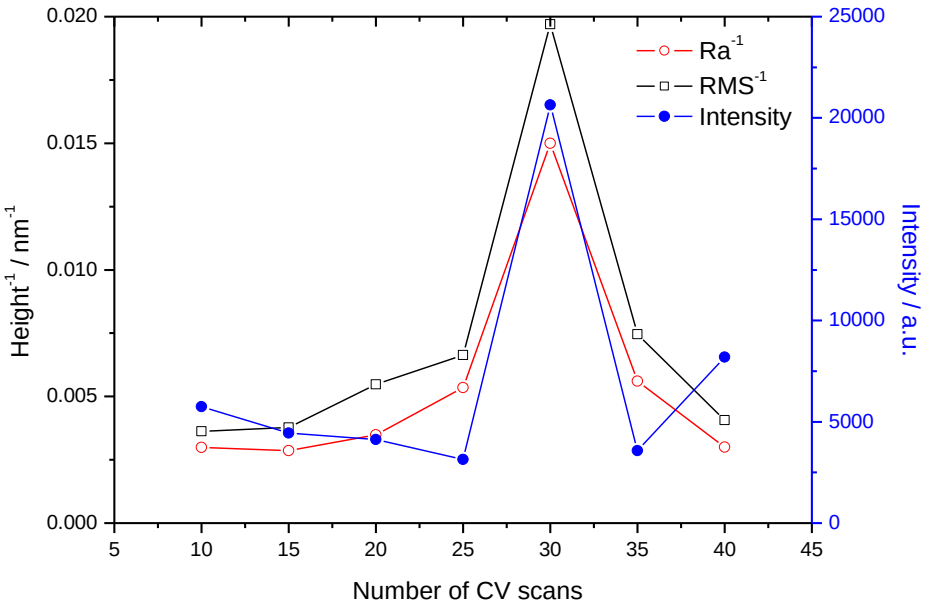

Figure 9. The variation of mean intensity of the Raman peak at 612 cm^{-1} and reciprocal value of amplitude parameters (RMS^{-1} and Sa^{-1}) with number of CV scans.

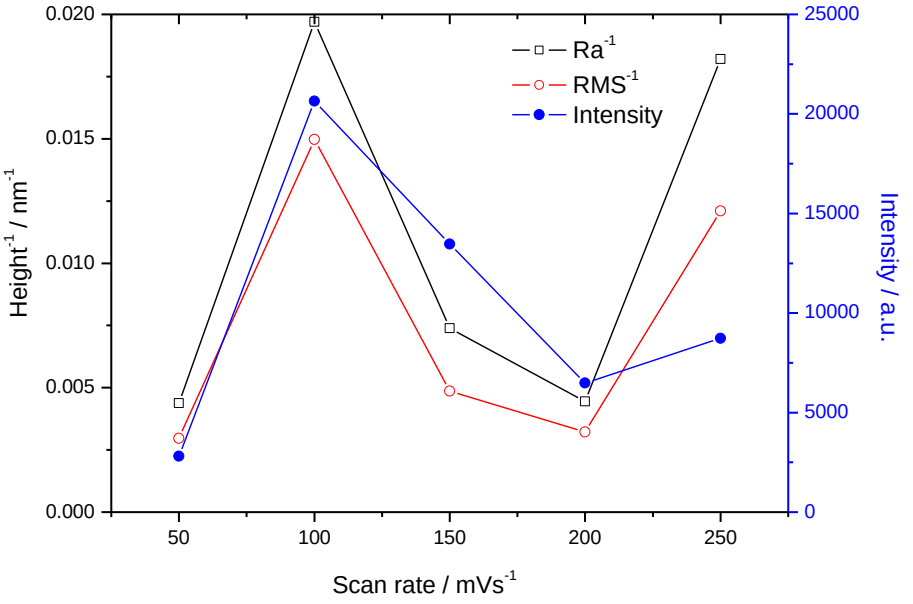

Figure 10. The variation of mean intensity of the Raman peak at 612 cm^{-1} and reciprocal value of amplitude parameters (RMS^{-1} and Sa^{-1}) with potential scan rate.

Effect of R6G concentration. Figure 11 shows the SERS spectra of R6G adsorbed on the Ag island SERS-active film prepared at the selected optimum preparation conditions (e.g. at potential scan rate 100 mV/s after 30 cycles) as a function of the concentration of R6G solution (ranging from 5×10^{-4} to 5×10^{-16} mol/l). The signal intensity increases gradually with rising concentration. Many bands are distinctly observed in the spectra even when the R6G concentration was reduced to 5×10^{-16} mol/l,

showing high sensitivity of the Ag nanoparticle film for SERS detection. A few Raman lines in the SERS spectra showed a good correlation with the concentration. The two most intense Raman peaks were taken for quantifying the relationship between the concentration of the R6G and the intensity of the Raman peak: at 612 cm^{-1} and at 1650 cm^{-1}.

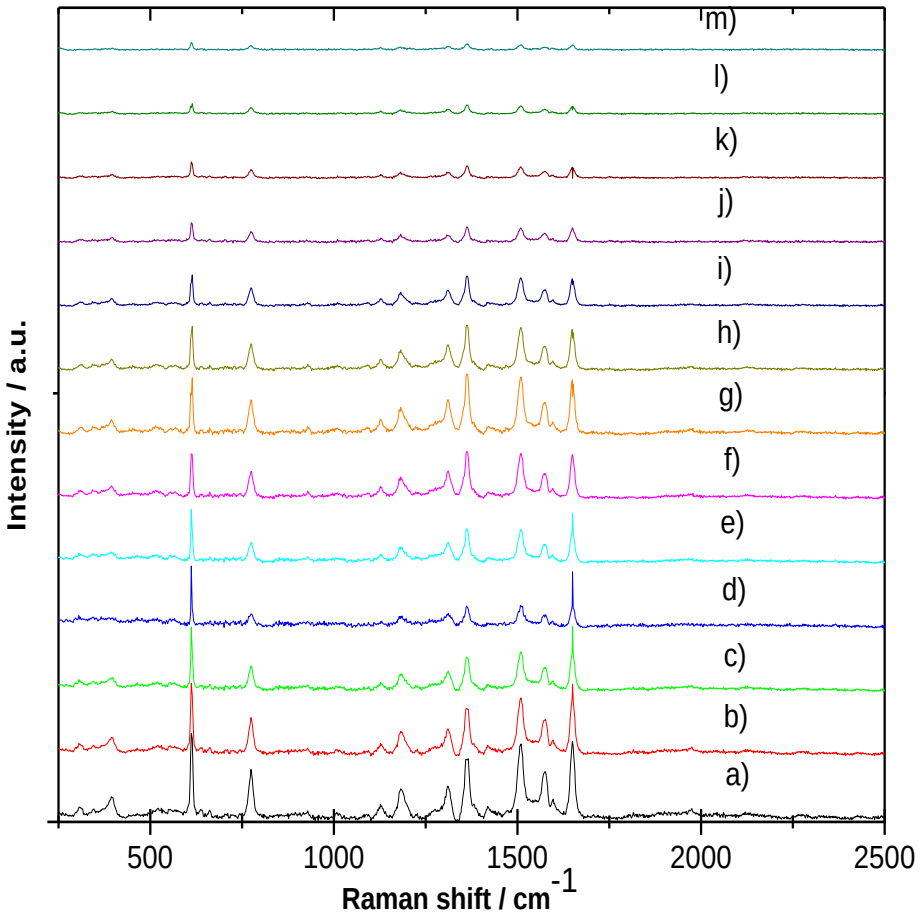

Figure 11. Representative SERS spectra of R6G adsorbed on Ag island films prepared by multiple scan CV at potential scan rate 100 mV/s after 30 cycles with different R6G concentrations: a) 5×10^{-4}; b) 5×10^{-5}; c) 5×10^{-6}; d) 5×10^{-7}; e) 5×10^{-8}; f) 5×10^{-9}; g) 5×10^{-10}; h) 5×10^{-11}; i) 5×10^{-12}; j) 5×10^{-13}; k) 5×10^{-14}; l) 5×10^{-15}; m) 5×10^{-16} mol/l.

Five additional substrates were prepared under selected optimum conditions (e.g. at potential scan rate 100 mV/s after 30 cycles) to evaluate the homogeneity and repeatability of the Ag film fabrication process. A total of ten measurements were made on each sample, at different locations, to calculate the mean and standard deviation of the two most intense Raman peaks of R6G (612 and 1650 cm^{-1}). The standard deviation deteriorated with a decreasing concentration. The RSD values less than 34 % (at higher concentrations less than 20%) (Table 3) demonstrate the excellent SERS activity and reproducibility and in turn also the good repeatability of the fabrication process as well the ability for the electrodeposition technique to control surface morphology.

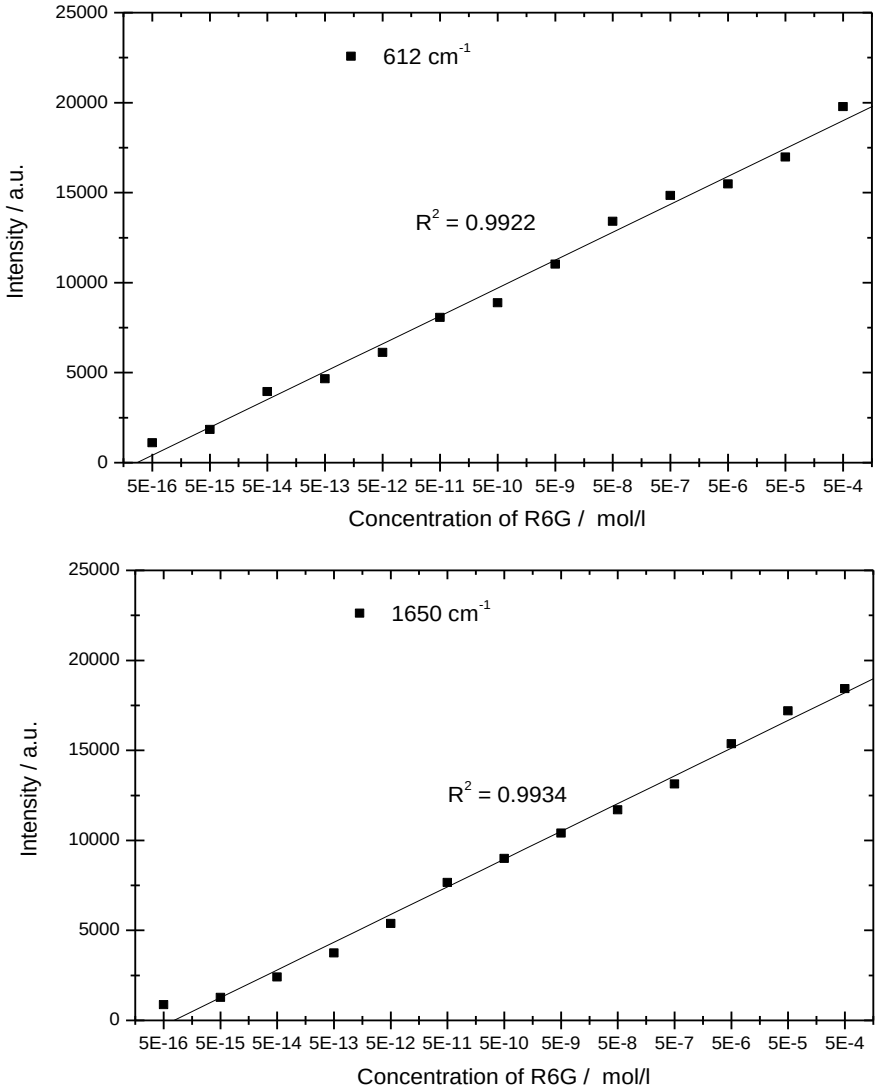

Figure 12. The variation of mean intensity of the Raman peak at 612 cm^{-1} and at 1650 cm^{-1} with R6G concentration.

Figure 12 shows the dependence of the mean value of the Raman peaks intensity of R6G adsorbed on the Ag island SERS-active film prepared at the selected optimum preparation conditions (e.g. at potential scan rate 100 mV/s after 30 cycles) at 612 cm^{-1} and 1650 cm^{-1} as a function of the concentration of R6G. The solid lines are the linear fits to the data. The intensity of both Raman bands varies linearly with the logarithmic concentration of R6G over a large concentration range of 12 orders of magnitude. Several factors may be responsible for this behaviour: lower number of R6G molecule effectively excited by the laser beam owing to not only a monolayer coverage of R6G molecules on the substrate and/or saturation of the surface at high concentration; chemical adsorption of major portion of R6G molecules on the Ag nanoparticles and so higher contribution from chemical enhancement, single R6G molecule - Ag nanoparticle interaction, and/or selective occupation of the "hot spots" until lower concentrations. The minimum detectable concentration was 5×10^{-16} mol/l. Corresponding intensities together with values of the determined analytical enhancement factor (*AEF*)

are summarized in Table 3. The larger standard deviations at lower concentrations could be attributed to the absence of chemical enhancement from some molecules as the spectra depend on the size and shape of the metal nanoparticles as well as on the orientation of adsorbed molecule on the metal nanoparticle or to the variation of R6G molecules number due to possible dilution inaccuracy and looseness during transfer to the substrate.

To estimate the enhancement ability of the Ag island film, the *AEF* was calculated. According to the method developed by Le Ru et al. [39], *AEF* is defined as follows:

$$AEF = \frac{I_{SERS}}{c_{SERS}} \frac{c_{RS}}{I_{RS}} \quad (1)$$

where I_{SERS} denotes the mean Raman intensity obtained for the Ag island nanoparticle SERS substrate under a certain concentration of c_{SERS}, and I_{RS} represents the Raman intensity obtained under non-SERS conditions on the stainless steel surface coated by continual smooth Ag layer with the thickness ~ 400 μm at the R6G concentration of $c_{RS} = 1\times10^{-3}$ mol/l. It was difficult to obtain an exact value of I_{RS} from non-Ag coated stainless steel surface due to strong fluorescence response. RS stands for "reference sample". In the present study I_{SERS} and I_{RS} were calculated using 612 and 1650 cm^{-1} as a reference peaks.

The prepared SERS-active substrate based on the optimum preparation conditions demonstrates a large *AEF* of 3.7×10^{12} (resp. 2.5×10^{12}) which significantly reduces the practical limit of detection of R6G to 5×10^{-16} mol/l. The number of the R6G molecules in 1 μl of solution at lower R6G concentration (5×10^{-16} mol/l) is: $5\times10^{-16} \times 10^{-6} \times 6.02\times10^{23} = 301$. The number of molecules actually illuminated by the laser beam should be lower.

Table 3. Values of mean intensity (*MI*) and relative standard deviation (*RSD*) of the Raman peak of R6G adsorbed on the Ag island SERS-active film prepared at the selected optimum preparation conditions (e.g. at potential scan rate 100 mV/s after 30 cycles) at 612 cm^{-1} and 1650 cm^{-1} together with the determined values of *AEF* as a function of the R6G concentration.

R6G concentration (mol/l)	612 cm^{-1}			1650 cm^{-1}		
	MI (a.u.)	*RSD* (%)	*AEF*	*MI* (a.u.)	*RSD* (%)	*AEF*
5×10^{-4}	1977 8	13.2	6.6×10^{1}	18426	11.4	5.3×10^{1}
5×10^{-5}	16981	11.1	5.7×10^{2}	17187	11.1	4.9×10^{2}
5×10^{-6}	15482	10.3	5.2×10^{3}	15369	11.5	4.4×10^{3}
5×10^{-7}	14849	10.7	5.0×10^{4}	13126	11.3	3.8×10^{4}
5×10^{-8}	13414	13.1	4.5×10^{5}	11691	14.1	3.4×10^{5}
5×10^{-9}	11031	16.4	3.7×10^{6}	10398	13.1	3.0×10^{6}
5×10^{-10}	8883	23.4	3.0×10^{7}	8990	21.7	2.6×10^{7}
5×10^{-11}	8062	17.7	2.7×10^{8}	7661	15.7	2.2×10^{8}
5×10^{-12}	6123	23.9	2.1×10^{9}	5389	23.2	1.5×10^{9}
5×10^{-13}	4657	22.5	1.6×10^{10}	3740	22.6	1.1×10^{10}
5×10^{-14}	3950	24.8	1.3×10^{11}	2402	27.4	6.9×10^{10}
5×10^{-15}	1848	30.8	6.1×10^{11}	1274	32.1	3.7×10^{11}
5×10^{-16}	1099	32.2	3.7×10^{12}	864	33.5	2.5×10^{12}

The detection of a single molecule adsorbed on Ag nanoparticle surfaces by SERS has attracted great interest [5, 40, 41]. Chemical reduction methods are generally used for the preparation of silver nanoparticle SERS-active substrates. Recently, electrochemical deposition has achieved success in the production of highly SERS active substrates for single molecule spectroscopy. Chang et al. have reported the preparation of SERS-active substrates by electrochemical deposition–dissolution cycles which demonstrated large Raman scattering enhancement for adsorbed R6G with an enhancement factor of 2.3×10^{8} and a limit of detection of 2×10^{-13} mol/l [5]. Huang et al. [12] have produced the patterned Ag nanoparticle films on patterned TiO_2 nanotube substrates through pulse-current electrodeposition. An enhancement factor of 1.3×10^{5} for pyridine on the Ag nanoparticle film was achieved. Ordered Ag nanowire arrays with high aspect ratio and high density self-supporting Ag nanowire patterns were successfully prepared by Sun et al. [8] using potentiostatic electrodeposition within the confined nanochannels of a commercial porous anodic aluminium oxide template. The maximum average SERS surface enhancement factor calculated for pyridine for multiple locations on these Ag nanowires was 2.2×10^{6}.

Our results show that Ag island films deposited onto a stainless steel substrate by multiple scan CV methods at the selected optimum preparation conditions act as very good SERS substrates for the ultra trace detection of R6G with an *AEF* of 3.7×10^{12} corresponding to a detection limit of 5×10^{-16} mol/l. Comparable results were reached with silver nanoclusters deposited on glass substrates using a magnetron cluster deposition system by Upender et al. [3]. The enhancement factor for R6G on prepared surfaces was 2×10^{12} corresponding to a detection limit of 10^{-16} mol/l.

The large SERS enhancement in Ag island film can be primarily ascribed to the local strong electromagnetic effect, which is associated with the resonance coupling between the adjacent Ag aggregates with multiple nanoparticles anchored on the stainless steel substrate surface. The higher density and closer gap regions between the interconnected Ag nanoparticle aggregates apparently allow the formation of "hot spots" in the film. Experiments have also demonstrated that these "hot spots" can lead to high Raman sensitivity and even single molecule detection limits [35, 42, 43].

Moreover, the aggregates have an increased number of SERS active sites due to the great number of nanoparticle junctions present so the type of surface shown in Figs. 3e and 6b offers many sites where the immobilised analyte molecules may sit between silver particles to give a substantial enhancement of SERS activity.

Furthermore, the nanoparticle substrates expose more crystal faces, which have higher free energies and facilitate efficient adsorption or binding of the analyte molecules onto the Ag island film surface, consequently enhancing the Raman signals by the CHEM effects [43, 44].

4. CONCLUSIONS

The silver island films were electrodeposited on a stainless steel substrate by controlling the scan rate of applied potential and electrodeposition cycles.

An increase in both size and density of the Ag nanoparticles with increasing number of deposition cycles was observed. A decrease in size and aggregation ability of Ag nanoparticles and

clusters, resulting in lower coverage of the working electrode, was registered with an increase in potential scan rate.

The strongest SERS effect was associated with the Ag nanoparticle films characterized by the best distribution, highest density and low size dispersion of nanoparticles. The significant enhancement of SERS activity was detected once the isolated structures become interconnected to form the uniformly distributed network providing many sites for analyte molecules.

The amplitude parameters of surface features were found to correlate inversely with the intensity value of R6G adsorbed on the Ag island nanoparticle film

The results suggest that the SERS enhancements arise from both the EM and CHEM effects. The large enhancement is mainly attributed to junctions of particle aggregates and is associated partly also with the unique surface properties, favouring interactions with analyte molecules.

The less than 20% RSD of the Raman intensity of the carbon skeleton stretching modes for the Ag nanoparticle film prepared at the selected optimum preparation conditions clearly demonstrated the high uniformity and reproducibility of the substrate as well good repeatability of the electrochemical fabrication process.

Ag island films deposited onto stainless steel substrate by multiple scan CV methods at the selected optimum preparation conditions (e.g. at potential scan rate 100 mV/s after 30 cycles) act as very good SERS substrates for the ultra trace detection of R6G with an *AEF* of 3.7×10^{12}, corresponding to a detection limit of 5×10^{-16} mol/l.

The presented Ag island films could improve the detection limit of R6G by four orders of magnitude as compared to previous reports dealing with the electrochemical fabrication of SERS active substrates. As the electrochemical deposition is very simple and inexpensive, it may be used in large-scale preparation of substrates that could be widely applied in Raman analysis.

ACKNOWLEDGEMENTS
Financial support from Grant VEGA No. 1/0211/12 of the Slovak Scientific Grant Agency is highly acknowledged.

References

1. M. E. Abdelsalam, P. N. Bartlett, J. J. Baumberg, S. Cintra, T. A. Kelf and A.E. Russell, *Electrochem. Comm.*, 7 (2005) 740.
2. I. M. I. Ismail, *J. Saudi Chem. Soc.*, 14 (2010) 351.
3. G. Upender, R. Satyavathi, B. Raju, K. Shadak Alee, D. Narayana Rao and C. Bansal, *Chem. Phys. Lett*,. 511 (2011) 309.
4. K. H. Yang, Y. Ch. Liu and Ch. Ch. Yu, *Electrochim. Acta,* 54 (2009) 4202.
5. Ch. Ch. Chang, K. H. Yang, Y. Ch. Liu and Ch. Ch. Yu, *Anal. Chimica Acta,* 709 (2012) 91.
6. Ch. Zhu, G. Meng, Q. Huang and Z. Huang, *J. Hazard. Mater.*, 211–212 (2012) 389.
7. M. Fan, G. F. S. Andrade and A. G. Brolo, *Anal. Chim. Acta*, 693 (2011) 7.
8. B. Sun, X. Jiang, S. Dai and Z. Du, *Mater. Lett.*, 63 (2009) 2570.
9. C. Jing and Y. Fang, *J. Colloid Interface Sci.*, 314 (2007) 46.
10. R. Sanci and M. Volkan, *Sensors Actuator B Chem.*, 139 (2009) 150.

11. Z. Lu, Y. Gu, J. Yang, Z. Li, W. Ruan, W. Xu, Ch. Zhao and B. Zhao, *Vib. Spectrosc.*, 47 (2008) 99.
12. Y. Huang, L. Sun, K. Xie, Y. Lai, B. Liu, B. Rena and Ch. Lin, *J. Raman Spectrosc.*, 42 (2011) 986.
13. E. Hao and G. C. Schatz, *J. Chem. Phys.*, 120 (2004) 357.
14. C .J. Orendorff, L. Gearheart, N. R. Jana and C. J. Murphy, *Phys. Chem. Chem. Phys.*, 8 (2006) 165.
15. M. Fleischmann, P. J. Hendra and A. J. McQuillan, *Chem. Phys. Lett.*, 26 (1974) 163.
16. R. Foucault, R. L. Birke and J. R. Lombardi, *Langmuir*, 19 (2003) 8818.
17. I. Baltog, N. Primeau, R. Reinish and J. L. Coutaz, *Appl. Phys. Lett.*, 66 (1995) 1187.
18. P. C. Lee and D. Meisel, *J. Phys. Chem.*, 86 (1982) 3391.
19. R. G. Freeman, K. C. Grabar, K. J. Allison, R. M. Bright, J. A. Davis, A. P. Guthrie, M. B. Hommer, M. A. Jackson, P. C. Smith, D. G. Walter and M. J. Natan, *Science*, 267 (1995) 1629.
20. Z. Q. Tian, B. Ren and D. Y. Wu, *J. Phys. Chem. B*, 106 (2002) 9463.
21. B. H. Loo, *J. Electroanal. Chem.*, 136 (1982) 209.
22. H. Yamada and Y. Yamamoto, *Surf. Sci.*, 134 (1983) 71.
23. R. De Mondt, K. Baert, I. Geuens, L. Van Vaeck and A. Hubin, *Langmuir*, 22 (2006) 11360.
24. J. D. Driskell, S. Shanmukh, Y. Liu, S. B. Chaney, X. J. Tang, Y. P. Zhao and R. A. Dluhy, *J. Phys. Chem. C*, 112 (2008) 895.
25. L. Wang, Y. Sun, G. Che and Z. Li, *Appl. Surf. Sci.*, 257 (2011) 7150.
26. C. Domingo, V. Resta, S. Sanchez-Cortes, J. V. Garcia-Ramos and J. Gonzalo, *J. Phys. Chem. C*, 111 (2007) 8149.
27. K. H. Yang, Y. C. Liu and C. C. Yu, *Langmuir*, 26 (2010) 11512.
28. M. Pagannone, L. G. Quagliano, L. Mattioli and G. Mattei, *J. Raman Spectrosc.*, 22 (1991) 825.
29. L. P. Bicelli, B. Bozzini, C. Mele and L. D'Urzo, *Int. J. Electrochem. Sci.*, 3 (2008) 356.
30. W. Wei, X. Mao, L. A. Ortiz and D. R. Sadoway, *J. Mater. Chem.*, 21 (2011) 432.
31. D. K. Sharma, A. Ott, A. P. O'Mullane and S. K. Bhargava, *Colloid Surface Physicochem. Eng. Aspect*, 386 (2011) 98.
32. Y. Chen, B. Dong and W. Zhou, *Appl. Surf. Sci.*, 257 (2010) 1021.
33. A. T. Dimitrov, S. Hadzijordanov, K. I. Popov, M. G. Pavlovic and V. Radmilovic, *J. Appl. Electrochem.*. 28 (1998) 791.
34. A. Gutes, C. Carraro and R. Maboudian, *ACS Appl. Mater. Interface*, 1 (2009) 2551.
35. Y. Lu, G. L. Liu and L. P. Lee, *Nano Lett.*, 5 (2005) 5.
36. Z. Sun, Y. Li, Y. Wang, X. Chen, J. Zhang, K. Zhang, Z. Wang, C. Bao, J. Zeng, B. Zhao and B. Yang, *Langmuir*, 23 (2007) 10725.
37. L. Jensen and G. C. Schatz, *J. Phys. Chem. A*, 110 (2006) 5973.
38. M. J. Natan, *Faraday Discuss.*, 132 (2006) 321.
39. E. C. Le Ru, E. Blackie, M. Meyer and P. G. Etchegoin, *J. Phys. Chem. C*, 111 (2007) 13794.
40. W. E. Doering and S. Nie, *J. Phys. Chem. B*, 106 (2002) 311.
41. P. Etchegoin, R. C. Maher, L. F. Cohen, H. Hartigan, R. J. C. Brown, M. J. T. Milton and J. C. Gallop, *Chem. Phys. Lett.*, 375 (2003) 84.
42. C. Cheng, B. Yan, S.M. Wong, X. Li, W. Zhou, T. Yu, Z. Shen, H. Yu and H. J. Fan, *Appl. Mater. Interfaces*, 2 (2010) 1824.
43. W. C. Zhang, X. L. Wu, C. X. Kan, F. M. Pan, H. T. Chen, J. Zhu and P. K. Chu, *Appl. Phys. A*, 100 (2010) 83.
44. A. M. Schwartzberg, C. D. Grant, A. Wolcott, C. E. Talley, T. R. Huser, R. Bogomolni and J. Z. Zhang, *J. Phys. Chem. B*, 108 (2004) 19191.